11. Tomkiewicz, Y.; Engler, E. M. *Bull. Am. Phys. Soc. B* **1975**, *20*, 479.
12. Tomkiewicz, Y.; Taranko, A. R. *Phys. Rev. B* **1978**, *18*, 733.
13. Tomkiewicz, Y. *EPR of Organic Conductor*; in *The Physics and Chemistry of Low Dimensional Solids*; by Alcacer. D. Reidel Pub. Comp. NATO Advanced Study Institute Series, 1980.
14. Mehring, M.; Spengler, J. *Phys. Rev. Lett.* **1984**, *53*, 2441.
15. Wheland, R. C.; Gillson, J. L. *Am. Chem. Soc.* **1976**, *98*, 3916.
16. Bozio, R.; Gilando, A.; Pecile, C. *Chem. Phys. Lett.* **1977**, *52*, 503.
17. Seidle, A. R.; Candela, T. F.; Finnegan, T. F.; Van Duyne, R. P.; Cape, T.; Kokoszka, G. F.; Woyciejes, P. M.; Hashmall, J. A. *Inorg. Chem.* **1981**, *20*, 2635.
18. Torrance, J. B.; Scott, B. A.; Welber, B.; Kaufman, F. B.; Seiden, P. E. *Phys. Rev. B.* **1979**, *19*, 730.
19. Bonai, R. D. R.; Brian, B. E.; Michael, A. H. *Inorganica Chimica Acta.* **1986**, *119*, 195.

Dissociative Recombination Rates of O_2^+ Ion with Low Energy Electrons

Jeonghee Seong and Hosung Sun*

Department of Chemistry, Pusan National University, Pusan 609-735 and Center for Molecular Science, KAIST, Taejon 305-701, Korea

Received August 21, 1996

The dissociative recombination of $O_2^+(v^+)+e^- \rightarrow O(^1S)+O(^1D)$ has been theoretically investigated using the multichannel quantum defect theory (MQDT). Cross sections and rate coefficients at various electron energies are calculated. The resonant structures in cross section profile, which are hardly measurable in experiments, are also determined and the existence of Rydberg states is found to affect the rates. The theoretical rate coefficients are computed to be smaller than experimental ones. The reasons for this difference are explained. The two-step MQDT procedure is found to be very useful and promising in calculating the state-to-state rates of the dissociative recombination reaction which is a very important and frequently found phenomenon in Earth's ionosphere.

Introduction

The capture of an electron by a positive ion (recombination) requires that the electron goes from a free to a bound state and thus, in some manner, gives off energy. The energy may be given to a third body or it may be radiated away as a result of free-bound transition. When the third body is the molecule (the positive ion combined with the incident electron) itself, the releasing energy can break the molecule into atomic fragments. This phenomenon is called dissociative recombination of an ion with an electron.

The green line of oxygen is observed in the night sky and in aurora. It was suggested that the oxygen green line which is a prominent feature of the spectrum of the night sky is due to the formation of the excited atom $O(^1S)$ through the dissociative recombination of O_2^+ ions with electrons1.

The following reaction produces the oxygen atom in the excited ^1S state

$$O_2^+ + e^- \rightarrow O(^1D) + O(^1S). \quad (1)$$

And, in the upper atmosphere, this $O(^1S)$ falls into the lower ^1D state and, consequently, the light of 5577 Å (green) is emitted.[2] Therefore, in astrophysics, it is of considerable interest to determine the recombination rates for production of excited oxygen atoms.

Zipf has measured the absolute intensities of ^1S(5577 Å) and ^1D(6300 Å) radiation coming out from the reaction (1) using a microwave afterglow apparatus.[3] By relating the decay of intensity to the measured decay of electron density, he obtained values for the partial rates; namely, $\alpha(^1S)=2.1\times 10^{-9}$ cm^3/sec and $\alpha(^1D)=1.9\times 10^{-7}$ cm^3/sec at 300 K. And his microwave afterglow results gave a quantum yield of 0.1 and 0.9 for $O(^1S)$ and $O(^1D)$, respectively.

During the last decade, in both laboratory and *in situ* atmospheric experiments the quantum yield of the excited states $O(^1S)$, $O(^1D)$, and $O(^1P)$ of oxygen atoms was explored.[4~11] And a review for the $O(^1S)$ quantum yields obtained from the satellite and rocket measurements was given by Yee *et al.*[12] Since the total rate as a function of ion vibrational level (v^+) has not been determined experimentally, the theoretical quantum yields for $v^+=1$ and 2 can test the assumption that the total rate is constant over v^+.

From a theoretical point of view, the dissociative recombination can be considered as an ion-electron collision process. So dynamic theories can be applied to this problem. Among those theoretical tools, multichannel quantum defect theory (MQDT) has been successful in investigating dissociative recombinations of H_2^+,[13~19] HD^+,[19] D_2^+,[19,20] CH^+,[21] and NO^+ ions[22~27] with low energy electrons.

MQDT[28~30] has brought a remarkable progress to theoreti-

cal studies of the dynamical processes involving infinite number of Rydberg states. Fano[31] first applied MQDT to a molecular system by using the idea of frame transformation. This theory was woven into a general collision theory by Chang and Fano.[32] Jungen and Atabek[20] extended the idea of frame transformation to rovibronic problems by introducing a transformation between the Born-Oppenheimer and the close-coupling descriptions.

The first application of MQDT to dissociative recombination was made by Giusti[33] using the "two-step treatment." This two-step method provides us with a unified treatment of the following two different interactions; rovibronic coupling between Rydberg and ionizing states, and electronic coupling between dissociative two-electron excited state and Rydberg (or ionizing) states. Giusti[16] first applied this theory to the dissociative recombination of H_2^+. Futhermore, Takagi *et al.*[21] reported rotational effect including a large rotational state dependence of cross sections. The theoretical cross section calculation with MQDT has proceeded recently for many molecules.[34~38]

We use a method based on MQDT which treats the direct and indirect process simultaneously, leading to complicated resonance structures in the cross section. We consider the dependence of cross sections on electronic coupling and quantum defect. And, direct and indirect cross sections and rates are both calculated.

In the following sections, we explain the dissociative recombination in detail and the O_2^+ ion system is defined. The background of multichannel quantum defect theory is reviewed. Step-by-step computational procedure is provided. The potential energy curves, quantum defect functions and electronic couplings used in this work are discussed. Cross sections and rates of the dissociative recombination reaction of O_2^+ ions with low energy electrons are given as results. An emphasis will be given to the electron temperature dependence of rates, to the role of Rydberg states, and to the initial vibrational level dependence of rates. Conclusions are provided in the last section.

Dissociative Recombination of O_2^+ Ion with Electron

The dissociative recombination of a diatomic molecular ion AB^+ can occur *via* a direct collision, that is,

$$AB^+ + e^- \rightarrow AB^{**} \rightarrow A + B. \quad (2)$$

In the above direct process, the positive ion AB^+ combined with the electron e^- (continuum state) is directly coupled to the repulsive state AB^{**}. The AB^{**} state is a doubly excited state of the neutral molecule AB. It is often called a resonant state or a superexcited state.

The formation of AB^{**} is most likely to occur when the nuclear separation is close to the value R_c, at which the difference between the potential curves for AB^{**} and AB^+ is equal to the incident electron energy. The R_c will be referred to as the capture point. At this point electron capture can occur without any simultaneous transfer of energy into nuclear motion.

After the formation of the AB^{**}, two things may happen. The repulsive force between the nuclei causes them to move apart and they may dissociate, trapping the extra electron. The recombination process is then complete. Alternatively an electron may be emitted through autoionization, the reverse of the process by which the electron is captured. The probability of autoionization rapidly decreases once the nuclei are further apart than the seperation point R_S at which the two potential curves (AB^+ and AB^{**}) cross. For this reason the seperation point RS is often also called the stabilization point.

The determination of the cross section of direct dissociative recombination involves the calculation of three quantities; the electronic coupling width between AB^+ and AB^{**}, the slope of the potential curve of AB^{**} at the singularity (at R_s), and the position of the capture point (R_c) of incoming electrons. In summary, in a direct recombination, the incident electron is directly captured to form the dissociative repulsive state AB^{**}. And the AB^{**} state is unstable so that it dissociates into atomic fragments of A and B.

Besides the direct dissociation recombination mentioned above, indirect dissociative recombination can also occur. There is a manifold of infinite neutral Rydberg states beneath the ionic state. Since these Rydberg states have a similar energy to that of the ion, the incident electron can be captured to the Rydberg state

$$AB^+ + e^- \rightarrow AB^* \rightarrow AB^{**} \rightarrow A + B. \quad (3)$$

Therefore there can exist an additional intermediate step, corresponding to electron capture in a Rydberg state AB^* associated with a vibrationally excited state of the initial ion AB^+. It is called indirect process.

In the first transition, a Rydberg state AB^* is formed in an excited vibrational level. This transition involves the transfer of energy from the incident electron directly to the vibrational motion of the nuclei. This initial capture step is followed by the predissociation of the state AB^*. This predissociation can be considered as a two-step process. The step $AB^* \rightarrow AB^{**}$ arises from configuration interaction between the Rydberg state AB^* and the dissociative state AB^{**}. If the potential energy curve associated with AB^{**} is repulsive, the nuclei will be forced apart and the recombination is completed by dissociation.

The most important feature of this indirect process is that the initial electron capture can occur only if the energy of the system coincides with the energy of a vibrational level of a Rydberg state. Thus for a given Rydberg state, one vibrational level at most will be important. Theoretical considerations show that the electron capture proceeds most easily when only one vibrational quantum is gained by the nuclear motion. This restricts our attention to those Rydberg states whose binding energies are just smaller than the vibrational spacing.

At high temperatures the indirect dissociative recombination process must always be less important for diatomic molecules than the direct dissociative recombination. At lower temperatures the indirect process could never be completely dominant, but it may have significant effects on the temperature dependence of the recombination rate below 500 K. The importance of the indirect process at low temperatures depends on the magnitude of the capture cross section and on whether or not there are Rydberg states whose first vibrational level lies just above the energy of the ion.

In the direct process, an incident electron is directly cap-

tured into the dissociative superexcited state. The repulsive interaction is the so called electronic coupling V(R) between electronic continuum and dissociative superexcited states. In the indirect process, an incident electron is captured into a Rydberg orbital by exciting a molecular ion rovibrationally and then the electronic coupling induces a transition from the Rydberg state to the dissociative superexcited state. The coupling among the infinite number of Rydberg states and the electronic continuum is the quantum defect function $\mu(R)$. Hence, this can be understood in terms of the relative importance of the following factors; R dependence of quantum defect, electronic coupling strength, and Franck-Condon factor between vibrational and dissociative states.

However, the two processes (direct and indirect) occur simultaneously. Because the potential energy curves of the initial molecular ion and the intermediate Rydberg states are very similar, any repulsive state of molecule which causes direct recombination will also lead to predissociation of the Rydberg state in indirect recombination. Therefore, we should consider both of the direct and the indirect processes.

We investigate the dissociative recombination of O_2^+ with electrons whose incident energy is in the range of 0.001 to 1 eV. The O_2^+ ion initially is in the ground electronic state of $X^2\Pi_g$. And the initial vibrational levels of O_2^+ considered are $v^+=0$, 1, and 2.

In this system, the atomic fragments are two neutral oxygen atoms. Among them the emphasis is given to the oxygen excited state of ^1S. Many observations and experiments were performed for this particular state.[39~45] Also it was verified that the most important dissociative state generating the ^1S of atomic oxygen should be $^1\Sigma_u^+$ superexcited state of neutral O_2. From the symmetry property, we immediately recognize that the Rydberg states which couple with the $^1\Sigma_u^+$ state of O_2 should also have a symmetry of $^1\Sigma_u^+$.

Therefore the dissociative recombination reactions considered in this work are as follows.[46]

$$\begin{aligned} &O_2^+(X^2\Pi_g;\ v^+=0,\ 1,\ \text{or}\ 2)+e^- \\ \rightarrow &O_2^*\ (^1\Sigma_u^+;\ \text{Rydberg}) \rightarrow O_2^{**}\ (^1\Sigma_u^+;\ \text{dissociative}) \\ &\rightarrow O(^1S)+O(^1D). \end{aligned}$$

For clarity, the dominant electronic configuration for each state is listed below:

O_2^+ ($X^2\Pi_g$) has a configuration of $1\sigma_g^2 1\sigma_u^2 2\sigma_g^2 2\sigma_u^2 3\sigma_g^2 1\pi_u^4 1\pi_g^1$, O_2 ($X^3\Sigma_g^-$) has a configuration of $1\sigma_g^2 1\sigma_u^2 2\sigma_g^2 2\sigma_u^2 3\sigma_g^2 1\pi_u^4 1\pi_g^2$, O_2^* ($^1\Sigma_u^+$; Rydberg) has a configuration of $1\sigma_g^2 1\sigma_u^2 2\sigma_g^2 2\sigma_u^2 3\sigma_g^2 1\pi_u^4 1\pi_g^1 np_\pi^1$ (np_π has a symmetry of π_u in terms of molecular orbital notation), and O_2^{**} ($^1\Sigma_u^+$; dissociative) has a configuration of $1\sigma_g^2 1\sigma_u^2 2\sigma_g^2 2\sigma_u^2 3\sigma_g^2 1\pi_u^4 1\pi_g^1 2\pi_u^1$.

Multichannel Quantum Defect Theory for Dissociative Recombination

The multichannel quantum defect theory (MQDT) provides a powerful tool for the study of the process involving highly excited (and continuum) states of molecules. The theory was first developed by Seaton[28] for atomic problems, and extended by Fano[47] to the coupling in molecules between electronic and nuclear rotational motions.

The MQDT approach to dissociative recombination was first introduced by Giusti.[33] She suggested the so called two-step procedure. In the first step, the vibrational coupling between core (in an ion) and external electron (incoming electron) is treated as a multichannel problem through the R dependence of the quantum defect. In the second step, the coupling between the Rydberg (and ionization) and dissociative state is treated as an electronic interaction through the R dependence of the electronic coupling. This method was later slightly modified by Nakamura *et al.*[25,48,49] In this work we adopt the Nakamura's method.

The basic concepts underlying the multichannel quantum defect method are as follows. The theory is an extension of the methods of collision theory into the range of negative electron energies where the scattered electron actually becomes a bound electron. When the principal quantum number n is large, the electron is likely to be found far away from the positively charged core, in a region where its classical motion is slow compared to the nuclear motion in the core. The point of view of collision theory can then be exploited by utilizing the *space-fixed* coordinate frame for the Rydberg electron and expanding the eigenfunction of the system in terms of the eigenstates of residual ion, characterized in a molecule by the vibrational (and rotational) quantum numbers $v^+(N^+)$ of the molecular core in its electronic state, say, $|n^+\Lambda^+\rangle$. As n decreases along a Rydberg series, a growing proportion of the probability amplitude of the Rydberg electron is contained in an inner region closer to the core. Here the strong Coulomb attraction causes the electron to move much faster than the nuclei so that the Born-Oppenheimer approximation becomes increasingly valid. In this limiting situation the Rydberg electron is more appropriately described in terms of the *molecule-fixed* coordinate system. The electron takes part in the rotational motion in the sense that it now has a well-defined orbital angular momentum component, Λ, along the rotating molecular axis. It also assists in determining the potential energy curve for nuclear vibrational motion which therefore differs somewhat from the curve of the ion: the vibrational wavefunctions are now $|v\rangle$ rather than $|v^+\rangle$.

First we consider all the short range interactions to build a reaction matrix K. A part of K matrix is associated with the electronic coupling V(R) between electronic continuum (called ionization channel which is formed by the attachment of incident electron to molecular ion) and discrete excited state (called dissociation channel which is essentially a dissociative state of neutral molecule).

From the perturbative Lippmann-Schwinger equation, we know that the K matrix is equal to the electronic coupling $V(R)$ in the first order approximation. That is,

$$K_{jj'}=\begin{cases} \langle\chi_{v^+}|V(R)|F_d\rangle_R \equiv \dfrac{\xi_{v^+}}{\pi} & \text{for } j=v^+ \text{ and } j'=d \\ 0 & \text{otherwise} \end{cases} \tag{4}$$

where χ_{v^+} is the vibrational wavefunction of the ion, d is the index for the dissociative superexcited state of the neutral molecule, and $F_d(R)$ represents the energy normalized nuclear radial wave function in the dissociation channel d.

The diagonalization of the K matrix yields the eigenchannels α with eigenphase shifts η_α,

$$\sum_j K_{jj'}U_{j'\alpha}=-\frac{1}{\pi}\tan\eta_\alpha\ U_{j\alpha} \tag{5}$$

$$\eta_\alpha=\pm\tan^{-1}\xi,\ \text{and}\ 0, \tag{6}$$

where

$$\xi^2=\sum_{v^+}\xi_{v^+}{}^2.$$

Here U is the unitary diagonalization matrix which should exist in eigenchannel function Ψ_α which is written as

$$\Psi_\alpha=\sum_{v^+}U_{v^+\alpha}\chi_{v^+}\Phi^+[f\cos(\pi\mu(R)+\eta_\alpha)-g\sin(\pi\mu(R)+\eta_\alpha)]$$
$$+U_{d\alpha}\Phi_d[F_d(R)\cos\eta_\alpha-G_d(R)\sin\eta_\alpha] \quad (7)$$

where Φ^+ and Φ_d are electronic wavefunction of the ion and the dissociative neutral state, respectively, f and g are regular and irregular Coulomb function, respectively. $G_d(R)$ is an irregular solution of the same nuclear Schr dinger equation as $F_d(R)$. Only the phase of $G_d(R)$ lags in phase by $\pi/2$. Note that η_α appears as an additional phase shift in each continuum asymptotic wave function due to the electronic interaction. $\mu(R)$ is a quantum defect function, which is included as a phase shift.

At this point we make use of the closure relation among the vibrational wave functions and account for the vibrational coupling. Then, we can write

$$\sum_{v^+}\chi_{v^+}(R)\,U_{v^+\alpha}\cos(\pi\mu(R)+\eta_\alpha)=\sum_{v^+}\chi_{v^+}\chi_{v^+}C_{v^+\alpha} \quad (8)$$

$$\sum_{v^+}\chi_{v^+}(R)\,U_{v^+\alpha}\sin(\pi\mu(R)+\eta_\alpha)=\sum_{v^+}\chi_{v^+}\chi_{v^+}C_{v^+\alpha} \quad (9)$$

The most basic quantities, C and S matrices, can be expressed as,

$$C_{v^+\alpha}=\sum_{v^+\alpha}U_{v^+\alpha}\langle\chi_{v^+}|\cos[\pi\mu_\Lambda(R)+\eta_\alpha]|\chi_{v^+}\rangle_R \quad (10)$$

$$C_{d\alpha}=U_{d\alpha}\cos\eta_\alpha \quad (11)$$

$$S_{v^+\alpha}=\sum_{v^+}U_{v^+\alpha}\langle\chi_{v^+}|\sin[\pi\mu_\Lambda(R)+\eta_\alpha]|\chi_{v^+}\rangle_R \quad (12)$$

$$S_{d\alpha}=U_{d\alpha}\sin\eta_\alpha. \quad (13)$$

The asymptotic wave function can now be written as

$$\Psi_\alpha=\sum_{v^+}\chi_{v^+}\Phi^+[fC_{v^+\alpha}-gS_{v^+\alpha}]+\Phi_d[F_d(R)C_{d\alpha}-G_d(R)S_{d\alpha}] \quad (14)$$

According to the procedure by Seaton, in order to obtain the scattering matrix, we introduce the matrices,

$$J^\pm=C\pm iS \quad (15)$$

$$X=J^+(J^-)^{-1} \quad (16)$$

$$R=i(1-X)(1+X)^{-1}. \quad (17)$$

Then the scattering matrix can be expressed as

$$\boldsymbol{S}=X_{oo}-X_{oc}\,(X_{cc}-e^{-2\pi i\nu})^{-1}\,X_{co}$$
$$=(1-i\boldsymbol{R})^{-1}\,(1+i\boldsymbol{R}), \quad (18)$$

where $\boldsymbol{R}$ is the reactance matrix given by

$$\boldsymbol{R}=R_{oo}-R_{oc}\,(\tan\pi\nu+R_{cc})^{-1}R_{co}. \quad (19)$$

The suffix $o(c)$ means the open (closed) channel; $R_{oc}(R_{cc})$ is the matrix of $I_o\times I_c(I_c\times I_c)$ with $I_c(I_o)$ the number of closed (open) channels. The open channels consist of one dissociative continuum and I_c-1 ionization continua corresponding to I_o-1 vibrational states of molecular ions. The closed channels are the vibrationally excited Rydberg states.

Finally, the dissociative recombination cross section $\sigma(v^+,\varepsilon)$ is given by

$$\sigma(v^+,\varepsilon)=g\frac{\pi}{k^2}\,|\,S_{dv^+}|^2, \quad (20)$$

where ε is the kinetic energy of incident electron. The multiplicity factor g is

$$g=\frac{[2-\delta(L_d,0)][2S_f+1]}{2(2S_i+1)}, \quad (21)$$

where, $2S_f+1$ is the spin multiplicity of the final channel d, $2S_i+1$ is the spin multiplicity of the initial channel v^+, L_d is the electronic angular momentum of the final dissociative state, δ is the Krϕnecker delta, and k is the electron wave number, *i.e.*, $\varepsilon=(\hbar^2/m)k^2$, and m is the electron mass.

We obtain the rate coefficient calculated from a Maxwellian average of the cross sections at an electron temperature T_e

$$\alpha_{v^+}(T_e)=(8/\pi mk^3T_e^3)^{1/2}\int\sigma_{v^+}(\varepsilon)\exp(-\varepsilon/kT_e)\varepsilon d\varepsilon \quad (22)$$

where the subscript v^+ indicates the vibrational state of initial ion, k is the Boltzmann constant, and $\alpha_{v^+}(T_e)$ is the dissociative recombination reaction rate at an electron temperature T_e.

Computations

Potential Energy Curves. The potential energy curves required in this work are those of the ground state ($X^2\Pi_g$) of O_2^+ ion and the dissociative superexcited state ($^1\Sigma_u^+$) of neutral O_2 molecule. The O_2^+ potential curve is obtained from the RKR fit of theoretical and experimental data by Krupenie.[50] The diabatic O_2 potential energy curve is basically taken from Guberman and Giusti-Suzor's work.[36] In the range of internuclear distance of $1.8\le R\le 3.0$ au, the potential curve of $^1\Sigma_u^+$ is that of Guberman and Giusti-Suzor's work.[36] And for $R>3.0$ au, a Morse potential curve is constructed from the spectroscopic data provided in the literatures.[36] The potential energy curves are presented in Figure 1, Table 1, and Table 2. In Table 1 the reference energy point for energy (R) (in cm^{-1}) is the $v^+=0$ level of O_2^+.

Using this O_2^+ ion potential energy curve, the vibrational wave functions χ_{v^+} for the v^+ level are numerically calculated. The potential energy curve for $O_2(^1\Sigma_u^+$; dissociative) is later utilized to determine the continuum wavefunctions of the atomic fragment $O(^1S)$.

Quantum Defect Functions. The quantum defect function defines the potential energy curves for a series of Rydberg states. As mentioned in the previous section, the partial wave of interest is orbital angular momentum $l=1$, *i.e.*, π_u orbital. A Rydberg electron is in this orbital. We obtained the quantum defect function $\mu(R)$ from Guberman and Giusti-Suzor's calculations.[36] The quantum defect is later used as the phase shift in scattering wavefunctions.

Electronic Couplings. The electronic coupling $V(R)$ between the electronic continuum and the dissociative state is given in the following terms,

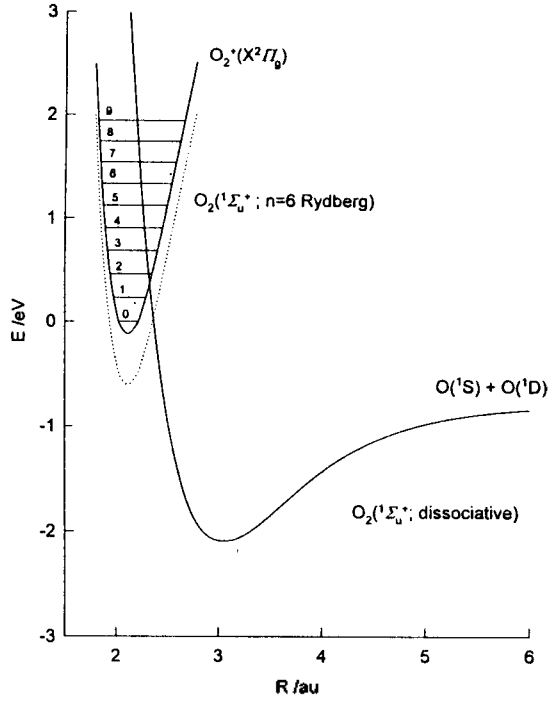

Figure 1. Potential energy curves of $O_2^+(X^2\Pi_g)$, $O_2(^1\Sigma_u^+$; Rydberg) and $O_2(1\Sigma_u^+$; dissociative) states. Vibrational levels of O_2^+ are also presented.

Table 1. Potential energy function of $O_2^+(X^2\Pi_g)$

Rau	Energy/cm^{-1}	R	Energy	R	Energy
1.786	20321.60	1.913	5520.01	2.442	7294.88
1.790	19568.49	1.925	4620.36	2.464	8170.11
1.795	18807.23	1.939	3712.57	2.486	9037.20
1.800	18037.84	1.955	2796.64	2.508	9896.14
1.805	17260.30	1.973	1872.57	2.529	10746.95
1.810	16474.63	1.996	940.35	2.550	11589.61
1.816	15680.81	2.028	0.00	2.570	12424.13
1.822	14878.85	2.051	−473.00	2.590	13250.51
1.828	14068.75	2.111	−948.69	2.610	14068.75
1.835	13250.51	2.177	−473.00	2.630	14878.85
1.841	12424.13	2.206	0.00	2.650	15680.81
1.848	11589.61	2.250	940.35	2.669	16474.63
1.856	10746.95	2.285	1872.57	2.689	17260.30
1.864	9896.14	2.316	2796.64	2.708	18037.84
1.872	9037.20	2.344	3712.57	2.727	18807.23
1.881	8170.11	2.370	4620.36	2.747	19568.49
1.891	7294.88	2.395	5520.01	2.766	20321.60
1.901	6411.52	2.419	6411.52		

$$\Gamma(R) = 2\pi\rho|V(R)|^2, \tag{23}$$

where ρ is a density of states and $\Gamma(R)$ is an electronic width. In our calculation, since we are using only one dissociative state, the density ρ is equal to unity. The $\Gamma(R)$ is taken from Guberman and Giusti-Suzor's work.[36] The width $\Gamma(R)$ is converted to $V(R)$ using Eq. (23). This $V(R)$ is later used

Table 2. Potential energy function of $O_2(^1\Sigma_u^+)$

For $1.80 \le R \le 3.20$ au

R/au	Energy/cm^{-1}	R	Energy	R	Energy
1.80	103951.48	2.27	7233.40	2.77	−15297.87
1.97	49528.36	2.37	−560.14	3.04	−16853.94
2.17	17614.56	2.57	−10506.73	3.20	−16694.93

For $3.20 \le R \le 10.0$ au

$D_e = 10557.8$ cm^{-1} $R_e = 3.073$ au $\beta = 1.33367$ au^{-1} $A = 1.000003513$

Energy(R) = A × 10557.8 × $(1.0 - e^{-\beta(R-Re)})^2$ − 16851.60

Table 3. Electronic coupling $V(R)$ and quantum defect function $\mu(R)$ taken from Ref. 36

R/au	$V(R)$/au	$\mu(R)$
1.80	0.0393	0.785
2.00	0.0432	0.737
2.20	0.0426	0.713
2.40	0.0383	0.704
2.60	0.0342	0.702
2.80	0.0301	0.703
3.00	0.0257	0.706

to determine the reactance matrix K and, subsequently, the eigenvectors U. Table 3 summarizes $V(R)$ and $\mu(R)$.

Computational Procedure. The step-by-step computational procedure is as follows[16,33]: i) Using the potential energy curve for O_2^+ ion, we calculate the vibrational wavefunctions (χ_{v^+}) for the $v^+ = 0$, 1, 2, etc. levels of O_2^+. At the same time vibrational energies are determined. In this work we calculate χ_{v^+} from $v^+ = 0$ to $v^+ = 6$ in order to include the couplings among many (open and closed) ionization channels. But rotational motions are not considered. ii) By setting the reactance matrix K equal to the electronic coupling $V(R)$ (first order approximation), we calculate phase shifts η_α and eigenfunctions U for the eigenchannel α. The K and U matrices are evaluated for various incident electron energies. The electron energy ε ranges from 0.001 to 1 eV. Since the K matrix varies slowly along the electron energy, K matrices are interpolated with the interval size of 0.0002 eV, whenever necessary. iii) The phase shifts due to the existence of Rydberg states are $\pi\mu(R)$. Since $\mu(R)$ is an input, it does not require any computations. iv) To determine the wavefunctions for atomic fragments, a single channel Schr dinger equation is solved using the potential energy curve of the dissociative $^1\Sigma_u^+$ state of O_2. v) With the phase shifts and wavefunctions computed in the previous steps, we construct an asymptotic atomic fragment wavefunction. And by comparing it with the initial bound wavefunction, we determine the C and S matrices. vi) With C and S matrices, X, R, and S matrices are evaluated. vii) Using Eq. (20), cross sections for each channel (v^+) are calculated. viii) By averaging the cross sections over various incident electron energies using Eq. (22), the dissociative recombination rate coefficients are calculated.

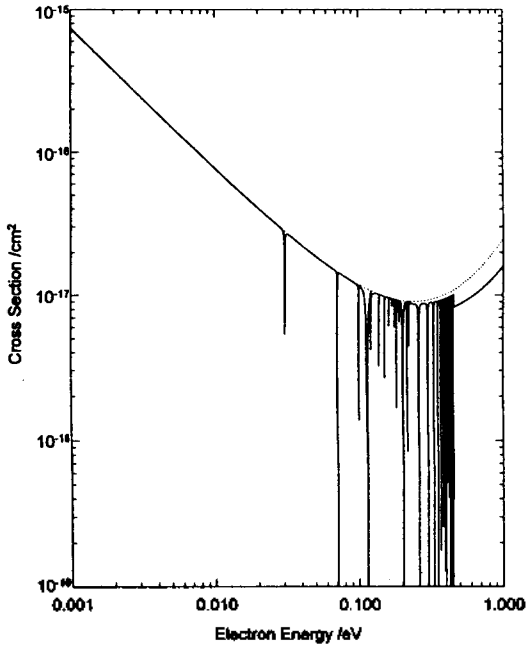

Figure 2. $v^+=0\rightarrow$*dissociation* cross sections with constant $\mu(R)=0.7198$(···; direct process).

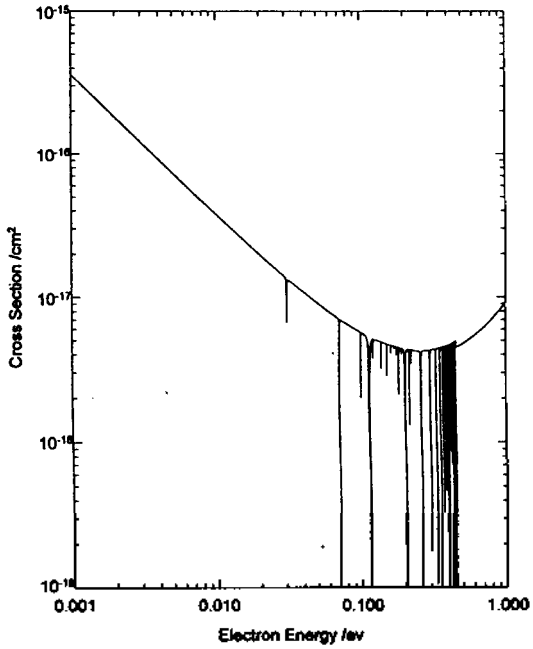

Figure 3. $v^+=0\rightarrow$*dissociation* cross sections with constant $\mu(R)=0.7198$ and constant $V(R)=0.0275$au.

Cross Sections and Rates

To understand the mechanism of dissociative recombination we have performed several tests. First, to see the direct process, the quantum defect function is set to be nil, *i.e.*, $\mu(R)=0$. It excludes the existence of all Rydberg states. And all the vibrational levels except for $v^+=0$ are excluded to get rid of vibrational-vibrational couplings between ionization channels. The cross sections for the recombination reaction of $O_2^+(v^+=0)+e^-\rightarrow O(^1D)+O(^1S)$ are presented in Figure 2. Here the dotted line indicates the cross sections for direct process. As expected the cross sections vary smoothly as the incident electron energy varies. In Figure 2, the abscissa indicates the incident electron energy in eV with respect to the $v^+=0$ level of O_2^+ ion. The ordimate indicates the cross sections in cm^2 for $v^+=0\rightarrow$*dissociation*. Both axes are in logarithmic scale.

The solid line in Figure 2 is the case for $\mu(R)$ being set to be nonzero constant (=0.7198). There we see many dips in cross sections. Each dip corresponds to a resonant Rydberg state. That is, an incident electron is captured to a certain vibrational level of Rydberg state of neutral O_2, where vibrational quantum number is usually one higher than that of O_2^+. And this state interacts with vibrational levels of O_2^+ and, later, electronic interaction with the dissociative $^1\Sigma_u^+$ state of O_2 leads it to dissociation fragments of oxygen atoms.

In second test, we set $V(R)$ to be constant (=0.0275au) as well as $\mu(R)$ (=0.7198). As shown in Figure 3, the shape of cross section profile is very similar to that of Figure 2. The difference is that the vibrational (*i.e.*, nuclear) motion of O_2^+ ion is homogeneous over R because $V(R)$ is constant.

In Figure 4, cross sections calculated with $V(R)=0.0275$au are presented. Here the quantum defect function $\mu(R)$ varies with the internuclear distance R. Comparing Figure 4 with

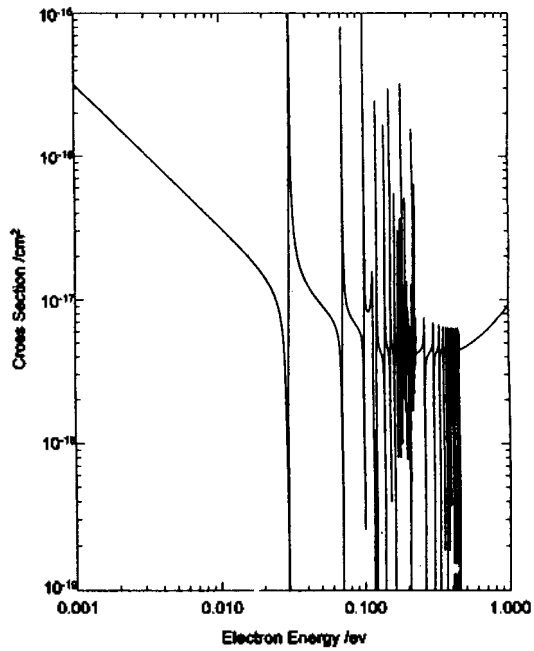

Figure 4. $v^+=0\rightarrow$*dissociation* cross sections with constant $V(R)=0.0275$au.

Figure 3, we immediately notice that the profile of cross section in Figure 3 changes a lot to a more complicated form. Each dip decreases and increases around matching electron energy with a certain Rydberg state. This kind of profile is called Fano-Beutler[51,52] shape. And the change of peak shape is due to the interaction between a bound state of O_2^+ ion (and of Rydberg O_2 state) and a continuum state (O_2^+ ion+electron). It implicitly indicates that our calculations correctly include the coupling between the Rydberg states and ion+electron continuum state.

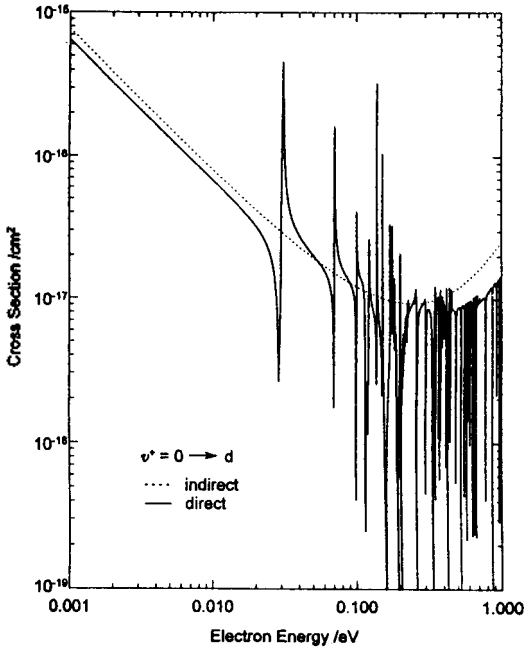

Figure 5. $v^+=0\rightarrow$*dissociation* cross sections (···; direct process).

From the above three tests (Figures 2, 3, and 4), we learn that the electronic coupling $V(R)$ plays the most important role in determining the dissociation cross section. And the quantum defect $\mu(R)$ causes a coupling between ionization channels (ion+electron continuum and vibrational state of Rydberg level) to generate many dips (sudden decrease of cross sections) in cross section profile. When $\mu(R)$ is not constant over R, the dip is changed to up-and-down shape as predicted by Fano.[52] The full cross sections for $v^+=0$ of O_2^+ to $O(^1S)$ dissociative recombination are presented in Figure 5.

As shown in Figure 5, at low electron energy, indirect cross sections are smaller than direct ones. It is because the incident electron is captured to a Rydberg state and stays at that state momentarily, which consequently delays the reaction. As expected, the overall cross sections decrease as the electron energy increases, because the electron having large kinetic energy is less likely to be drawn by the attractive Coulombic force of O_2^+ positive ion. But at very large electron energies, the cross sections become larger as the electron energy becomes larger, because there are more channels becoming open when the electron energy is very large.

Though we do not present detailed results, we have also performed similar type of calculations for $v^+=1\rightarrow$*dissociation* and $v^+=2\rightarrow$*dissociation* processes. The same characteristics of recombination process obtained from $v^+=0\rightarrow$*dissociation* calculations are also found in $v^+=1$ and $v^+=2$ calculations.

Experimentally the up and down structures (resonant structures due to Rydberg states) in cross sections do not manifest because of the wide distribution of incident electron energy (low resolutions). Rather the Maxwell-Boltzmann average of electron energy is accounted for smooth cross section profile. Therefore using Eq. (22) we have calculated the rate coefficients. It is customary to report incident electron kinetic energy in terms of temperature, T_e. The rate coefficient dependency on T_e is expressed as closed formula like those in Table 4.

Table 4 shows the dissociative recombination rate coefficients for $O_2^+(v^+)+e^-\rightarrow O(^1S)+O(^1D)$. Indirect process means that the couplings between ionization channels and Rydberg states of O_2 are also included in addition to the couplings between ionization channels and dissociative state of O_2 (direct process). The rate coefficients decrease as the T_e increases in the range of $T_e=100$ to 1000 K. For $v^+=0\rightarrow$*dissociation* process, indirect rate coefficients are larger than direct rate coefficients. For $v^+=1$ or $2\rightarrow$*dissociation* process, indirect rate coefficients are smaller than direct rate coefficients. We also note that the rate coefficient for $v^+=2\rightarrow$*dissociation* is largest and that for $v^+=0\rightarrow$*dissociation* is smallest among the three channels. For example, at $T_e=300$ K, α ($v^+=0\rightarrow$*dissociation*)$=2.62\times10^{-8}$ cm^3/s, α ($v^+=1$)$=7.22\times10^{-9}$ cm^3/s, α ($v^+=0$)$=4.42\times10^{-10}$ cm^3/s from indirect process calculations.

The entry denoted as GS in Table 4 is the theoretical work by Guberman and Giusti-Suzor.[36] In their work they used a basically identical MQDT theory as ours. And the same set of electronic coupling and quantum defect functions are used actually because our values are taken from their work. The difference between two calculations lies in the form of potential curves of O_2^+ ground state and O_2 dissociative state, but, overall, the difference is not so critical. As we see in Table 4, our rate coefficients agree to those by Guberman and Giusti-Suzor (GS) within an order of magnitude. GS's α ($v^+=2\rightarrow$*dissociation*) is also largest among three α's. Some years ago Guberman reported the direct process

Table 4. Rate coefficients (cm^3/s) for $O_2^+(v^+)+e^-\rightarrow O(^1S)+O(^1D)$

	This work		GS[a]
v^+	Direct	Indirect	
$200\le T_e\le400$ K			
0	$3.54\times10^{-10}(T_e/300)^{-0.37}$	$4.42\times10^{-10}(T_e/300)^{-0.21}$	$2.30\times10^{-10}(T_e/300)^{-0.13}$
1	$9.45\times10^{-9}(T_e/300)^{-0.42}$	$7.22\times10^{-9}(T_e/300)^{-0.57}$	$2.40\times10^{-9}(T_e/300)^{-0.51}$
2	$4.33\times10^{-8}(T_e/300)^{-0.48}$	$2.62\times10^{-8}(T_e/300)^{-0.43}$	$1.40\times10^{-8}(T_e/300)^{-0.69}$
$600\le T_e\le1000$ K			
0	$2.77\times10^{-10}(T_e/800)^{-0.92}$	$3.33\times10^{-10}(T_e/800)^{-0.33}$	$2.10\times10^{-10}(T_e/800)^{-0.17}$
1	$6.66\times10^{-9}(T_e/800)^{-0.28}$	$4.70\times10^{-9}(T_e/800)^{-0.32}$	$3.10\times10^{-9}(T_e/800)^{-0.07}$
2	$2.72\times10^{-8}(T_e/800)^{-0.47}$	$1.84\times10^{-8}(T_e/800)^{-0.35}$	$7.90\times10^{-8}(T_e/800)^{-0.52}$

[a] Ref. 36 (theoretical work)

calculations of for $v^+=0$, 1, 2, 3, and 4→*dissociation*.[37,38] In the calculations, he also found α ($v^+=2$→*dissociation*) is largest (larger than α ($v^+=3$) or α ($v^+=4$)). The theoretically calculated quantum yields for O_2^+ ($v^+=0$ only)$+e^-\rightarrow O(^1D)+O(^1S)$, at $T_e=300$ K, are 0.0021 (indirect process in this work), 0.0011 (GS), and 0.0016 (Guberman). Zipf[53] reported that experimental quantum yield for $O_2^+(v^+=0, 1, 2, 3$ all$)+e^-\rightarrow O(^1D)+O(^1S)$ is 0.02. Here we note that the experimental quantum yield is at least 10 times larger than any theoretical quantum yield. The theoretical quantum yield for O_2^+ ($v^+=1$ only)→*dissociation* and $O_2^+(v^+=2$ only) are 10 or 100 times larger than that for $O_2^+(v^+=0$ only). Therefore the very large experimental quantum yield can be explained if the O_2^+ ion is initially in some vibrationally excited states. Actually Zipf[54] determined the initial vibrational distribution of O_2^+ ion using Guberman's theoretical quantum yields and his experimentally measured quantum yields. But, on the other hand, there is an evidence that the vibrationally excited O_2^+ ion can be easily quenched to the ground $v^+=0$ level by a collision with atomic oxygen.[10] If so, the excited vibrational level of O_2^+ can not be heavily populated so that most O_2^+ ions should be in the ground state initially.

In other experiments,[55,56] the rate coefficients for $O_2^+(v^+=0)+e^-\rightarrow 2O$ (in any state) are found to be 1.95×10^{-7} cm^3/s at $T_e=300$ K. It corresponds to the quantum yield of 0.93, which is again very larger than any theoretical value. Therefore, as Guberman and Giusti-Suzor argued,[36] we also believe that theoretical rate coefficients or quantum yields are much smaller than experimental ones. We do not know the exact reason why theory gives smaller quantum yields than experiment. The possible reasons for this discrepancy, we learn from this work, are: i) The diabatic potential curve of dissociative state used in the theoretical work crosses near the point (R_c) of $v^+=2$ vibrational level of O_2^+ ion potential curve (see Figure 1). So it is natural that $\alpha(O_2^+(v^+=2))$ is largest. Hence $\alpha(O_2^+(v^+=0))$ is smaller. ii) The internuclear distance dependency of electronic coupling, used in the theoretical work, is too much delocalized, *i.e.*, as seen in Table 3, over the range of $R=1.8$ to 3.0au the electronic coupling is consistently large. Electronic coupling should be largest near the crossing point and diminishes away from the crossing point. Instead of first order approximation of Lippmann-Schwinger equation (see Eq. 4), more accurate second order approximation can be used, but this second order calculation[36] did not account for the discrepancy. iii) The relevant dissociative state could be more than one. The $^1\Sigma_u^+$ state used in this work could be only one of them. The more dissociative states are involved, the larger the rate coefficients are.

Conclusions

The dissociative recombination of $O_2^+(v^+)+e^-\rightarrow O(^1S)+O(^1D)$ has been theoretically investigated using the multichannel quantum defect theory. Cross sections and rate coefficients at various electron energies are calculated. The resonant structures in cross section profile, which are hardly measurable in experiments, are determined. Therefore the role of Rydberg manifold is found to be non-negligible.

The theoretical rate coefficients are found to be smaller than the experimental ones. The reason for this difference should be examined in future works. However we learn that, in theory, more accurate potential curves and electronic couplings should be used. And, in experiments, the initial vibrational state of O_2^+ ion should be determined beforehand.

Nonetheless the two-step MQDT procedure adopted in this work is found to be very useful and promising in calculating the state-to-state rates of dissociative recombination reaction which is a very important and frequently found phenomenon in Earth's ionosphere. In the future theoretical efforts to determine accurate potential curves, quantum defect function and particularly electronic coupling should continue.

Acknowledgment. The present study was supported, in part, by the Basic Science Research Institute Program, Ministry of Education, Korea, 1995, Project No. BSRI-95-3409.

References

1. Kaplan, J. *Phys. Rev.* **1931**, *38*, 1048.
2. Nicolet, M. *Phys. Rev.* **1954**, *93*, 633.
3. Zipf, E. C. *Bull. Am. Phys. Soc.* **1970**, *15*, 418.
4. Abreu, V. J.; Solomon, S. C.; Sharp, W. E.; Hays, P. B. *J. Geophys. Res.* **1983**, *88*, 4140.
5. Killeen, T. L.; Hays, P. B. *J. Geophys. Res.* **1983**, *88*, 10163.
6. Fox, J. L.; Bougher, S. W. *Space Sci. Rev.* **1991**, *55*, 357.
7. Zipf, E. C. *Geophys. Res. Lett.* **1979**, *6*, 881.
8. Bates, D. R. *Planet. Space Sci.* **1992**, *40*, 211.
9. Bates, D. R. *Planet. Space Sci.* **1990**, *38*, 889.
10. Bates, D. R.; Zipf, E. C. *Planet. Space Sci.* **1980**, *28*, 1081.
11. Alge, E.; Adams, N. G.; Smith, D. *J. Phys. B: At. Mol. Phys.* **1983**, *16*, 1433.
12. Yee, J. H. *Planet. Space Sci.* **1988**, *36*, 89.
13. Hickman, A. P. *J. Phys. B: At. Mol. Phys.* **1987**, *20*, 2091.
14. O'Malley, T. F. *J. Phys. B: At. Mol. Phys.* **1981**, *14*, 1229.
15. Schneider, I. F.; Dulieu, O.; Giusti-Suzor, A. *J. Phys. B: At. Mol. Phys.* **1991**, *24*, 1289.
16. Giusti-Suzor, A.; Bardsley, J. N.; Derkits, C. *Phys. Rev. A* **1983**, *28*, 682.
17. Ross, S.; Jungen, Ch. *Phys. Rev. Lett.* **1987**, *59*, 1297.
18. Tennyson, J.; Noble, C. J. *J. Phys. B: At. Mol. Phys.* **1985**, *18*, 155.
19. Nakashima, K.; Takagi, H.; Nakamura, H. *J. Chem. Phys.* **1987**, *86*, 726.
20. Jungen, Ch.; Atabek, O. *J. Chem. Phys.* **1977**, *66*, 5584.
21. Takagi, H.; Kosugi, N.; Le Dourneuf, M. *J. Phys. B: At. Mol. Phys.* **1991**, *24*, 711.
22. Dulaney, J. L.; Biondi, M. A.; Johnsen, R. *Phys. Rev. A* **1987**, *6*, 1352.
23. Bardsley, J. N. *Planet. Space Sci.* **1983**, *31*, 667.
24. Giusti-Suzor, A.; Jungen, Ch. *J. Chem. Phys.* **1984**, *80*, 986.
25. Sun, H.; Nakamura, H. *J. Chem. Phys.* **1990**, *93*, 6491.
26. Lee, C. M. *Phys. Rev.* A **1977**, *16*, 109.
27. Raoult, M. *J. Chem. Phys.* **1987**, *87*, 4736.
28. Seaton, M. J. *Proc. Phys. Soc. London* **1966**, *88*, 801.
29. Seaton, M. J. *Rep. Prog. Phys.* **1983**, *46*, 167.
30. Greene, C. H.; Jungen, Ch. *Adv. Atom. Mol. Phys.* **1985**, *21*, 1.
31. Fano, U. *Phys. Rev.* A **1970**, *2*, 353.
32. Chang, E.; Fano, U. *Phys. Rev.* A **1972**, *6*, 173.
33. Giusti, A. *J. Phys. B: At. Mol. Phys.* **1980**, *13*, 3867.
34. Bates, D. R. *J. Phys. B: At. Mol. Phys.* **1992**, *25*, 5479.

35. Giusti-Suzor, A.; Lefebvre-Brion, H. *Phys. Rev.* A **1984**, *30*, 3057.
36. Guberman, S. L.; Giusti-Suzor, A. *J. Chem. Phys.* **1991**, *95*, 2602.
37. Guberman, S. L. *Nature* **1987**, *327*, 408.
38. Guberman, S. L. *Can. J. Phys.* **1986**, *64*, 1621.
39. Saxon, R. P.; Liu, B. *J. Chem. Phys.* **1977**, *67*, 5432.
40. Katsumata, S.; Kimura, K. *Appl. Spectro. Rev.* **1992**, *27*, 193.
41. Guberman, S. L. *Int. J. Quantum Chem.* **1979**, *S13*, 531.
42. Guberman, S. L. *Physics of Ion-Ion and Electron-Ion Collisions*; Brouillard, F.; McGowan, J. Wm., Ed.; Plenum: New York, 1983; pp 167-200.
43. Guberman, S. L. *Dissociative Recombination: Theory, Experiment, and Applications*; Mitchell, J. B. A.; Guberman, S. L., Ed.; World Scientific: Singapore, 1989; pp 45-60.
44. Mitchell, J. B. A.; McGowan, J. Wm. *Physics of Ion-Ion and Electron-Ion Collisions*; Brouillard, F.; McGowan, J. Wm., Ed.; Plenum: New York, 1983; pp 279-324.
45. Michels, H. H. *The Excited State in Chemical Physics Part 2*; McGowan, J. Wm., Ed.; Plenum: New York, 1981; pp 225-340.
46. Mulliken, R. S.; Ermler, W. C. *Diatomic Molecules*; Academic Press: New York, 1977.
47. Fano, U. *Phys. Rev.* A **1978**, *17*, 93.
48. Nakamura, H. *J. Phys. Chem.* **1984**, *88*, 4812.
49. Takagi, H.; Nakamura, H. *J. Chem. Phys.* **1981**, *74*, 5808.
50. Krupenie, P. H. *J. Phys. Chem. Ref. Data* **1972**, *1*, 423.
51. Beutler, H. *Z. Physik* **1935**, *93*, 177.
52. Fano, U. *Phys. Rev.* **1961**, *124*, 1866.
53. Zipf, E. C. *J. Geophys. Res.* **1980**, *85*, 4232.
54. Zipf, E. C. *Planet. Space Sci.* **1988**, *36*, 621.
55. Alge, E.; Adams, N. G.; Smith, D. *J. Phys. B: At. Mol. Phys.* **1983**, *16*, 1433.
56. Mehr, F. J.; Biondi, M. A. *Phys. Rev.* **1969**, *181*, 264.